Bull. Mater. Sci., Vol. 34, No. 3, June 2011, pp. 525–529. © Indian Academy of Sciences.

Processing maps for Fe–24Ni–11Cr–3Ti–1Mo superalloy

CAI DAYONG*, ZHANG CHUNLING, TANG ZHIGUO, DONG HAIFENG and WANG PENG
State Key Laboratory of Metastable Materials Science & Technology, Yanshan University, Qinhuangdao 066004, Hebei, China

MS received 10 March 2009; revised 21 February 2011

Abstract. Hot deformation characteristics of a Fe-base superalloy were studied at various temperatures from 1000–1200°C under strain rates from 0·001–1 s^{-1} using hot compression tests. Processing maps for hot working are developed on the basis of the variations of efficiency of power dissipation with temperature and strain rate and interpreted by a dynamic materials model. Hot deformation equation was given to characterize the dependence of peak stress on deformation temperature and strain rate. Hot deformation apparent activation energy of the Fe–24Ni–11Cr–1Mo–3Ti superalloy was determined to be about 499 kJ/mol. The processing maps obtained in a strain range of 0·1–0·7 were essentially similar, indicating that strain has no significant influence on it. The processing maps exhibited a clear domain with a maximum of about 40–48% at about 1150°C and 0·001 s^{-1}.

Keywords. Superalloy; hot deformation; efficiency of power dissipation; processing maps.

1. Introduction

Fe–24Ni–11Cr–1Mo–3Ti alloy is an age hardened Fe-base superalloy with excellent low thermal expansion property at high temperatures. The alloy containing 3wt% Ti and 0·5wt% Al is strengthened by fine precipitation of the γ' (Ni_3AlTi) phase in the matrix by aging after solution heat treatment, also including the solid solution hardening of Mo and grain boundary hardening of B. The alloy possesses heat resisting properties up to about 700°C. The low cost and excellent working properties resulted in it being widely applied in gas turbine as high temperature attaching parts and spring (Kusabiraki *et al* 1996, 1997, 1998). Since these components withstand high alternating stresses and creep loads, uniform microstructure with fine grains must be obtained by controlling forging processes. The maximum limit of temperature for effective use increases with the complexity of the alloy and the phase present in it. Thus, the alloying additions and the phases present in the matrix greatly influence the hot workability of the alloy. The workability of a material is specified by its flow stress, which depends on the deformation temperature and strain rate.

Processing maps were developed on the basis of the dynamic material model (Raj 1981; Omar *et al* 1996; Park *et al* 2002). The model considers the work piece as a dissipater of power and that the instantaneous power dissipated at a given strain rate ($\dot{\varepsilon}$) consists of two complementary parts: the G content and the J co-content, representing the temperature rise and the microstructural dissipation, respectively. The factor that partitions the power between J and G is the strain-rate sensitivity (m) of the flow stress (σ), the J co-content being given by

$$J = \sigma \cdot \dot{\varepsilon}\, m/(m+1), \tag{1}$$

where $\dot{\varepsilon}$ is the strain rate. For an ideal linear dissipater, $J = J_{\max} = \sigma \cdot \dot{\varepsilon}/2$. For a non-linear dissipater, the efficiency of power dissipation may be expressed in terms of a dimensionless parameter:

$$\eta = 2m/(m+1). \tag{2}$$

The variation in η with temperature and strain rate constitutes the power dissipation map, the domains of which may be interpreted in terms of specific microstructural processes (Somani *et al* 1995; Srinivasan and Prasad 1995; Chakravartty *et al* 1995; Seshacharyulu *et al* 2000; Balasubrahmanyam and Prasad 2002).

The processing map is very beneficial for optimizing hot workability and controlling microstructure in the material. With the help of a processing map, it is possible to arrive at the optimum parameters for designing a metal working process without resorting to expensive and time-consuming trial and error methods. The aim of the present investigation was to develop processing maps for hot working of the Fe–24Ni–11Cr–1Mo–3Ti superalloy, with a view to understanding the constitutive behaviour of the material under hot working conditions.

2. Experimental

The chemical composition of Fe–24Ni–11Cr–1Mo–3Ti superalloy used in this study is shown in table 1.

*Author for correspondence (cdy@ysu.edu.cn)

Table 1. Chemical composition of Fe–24Ni–11Cr–1Mo–3Ti superalloy (mass%).

C	Ni	Cr	Mo	Ti	Al	B	Mn	Fe
0·04	23·6	11·4	1·37	3·02	0·49	<0·001	≤0·10	Balance

Hot-compression tests were conducted using Gleeble-3500 simulator at various temperatures from 1000–1200°C under strain rates from 0·001 to 1 s^{-1} with cylindrical specimens of 10 mm diameter and 15 mm height. All specimens were quickly heated to 1200°C and held for about 5 min in order to gain a uniform microstructure before the hot compression test. After that they were cooled to hot compression temperature with a cooling rate of 10°C/s and held for 2 min, and then deformed to a true strain of 0·7, immediately followed by water quenching. The deformed specimens were sectioned parallelly to the compression axis and the cut surfaces were prepared for microstructure observation.

The load-stroke data obtained in compression were processed to obtain true stress–true plastic strain curves using the standard method. The efficiency of power dissipation (η) through microstructural changes was then calculated as a function of temperature and strain rate using (1) and plotted as an iso-efficiency contour map.

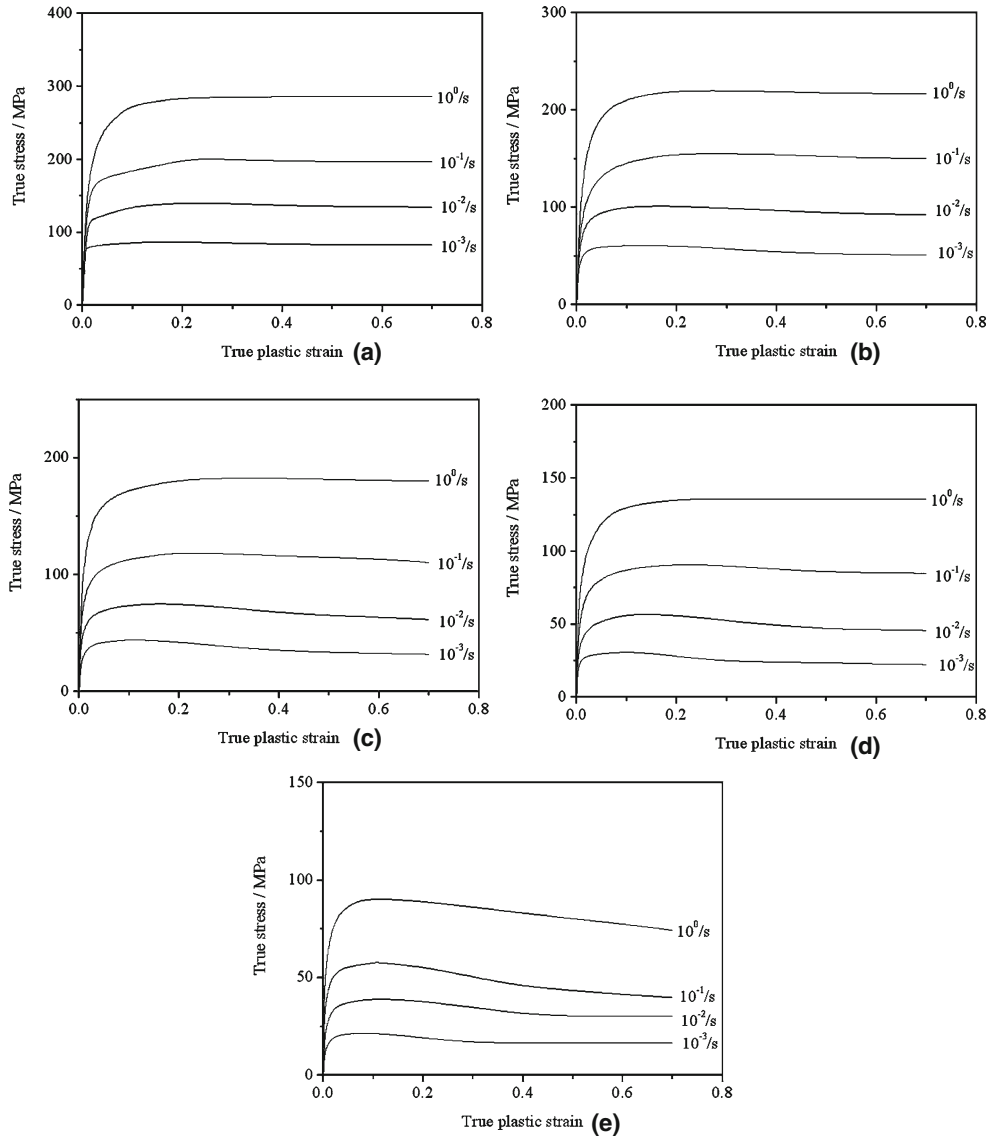

Figure 1. True stress–true strain flow curves for Fe–24Ni–11Cr–1Mo–3Ti superalloy under different strain rates and temperatures: (**a**) 1000°C, (**b**) 1050°C, (**c**) 1100°C, (**d**) 1150°C and (**e**) 1200°C.

3. Results and discussion

3.1 *True stress–true plastic strain curves*

A series of typical stress–strain curves of the Fe–24Ni–11Cr–1Mo–3Ti superalloy deformed at various temperatures from 1000–1200°C under strain rates from 0·001–1 s^{-1} is shown in figure 1. At low temperatures and high strain rates, the flow stress increases rapidly with the increase of strain and then reaches a steady state. Conversely, at high temperatures and low strain rates, the flow stress increases to a peak value with the increase of strain and then decreases as the strain further increased. The initial rapid rise in stress is associated with the increase of dislocation density and the formation of subgrain boundaries, as a result of work hardening and dynamic recovery. The high dislocation density stimulates the occurrence of dynamic recrystallization once a critical strain is exceeded.

3.2 *Development of constitutive relationship*

The peak stress can be selected as the representative stress of each curve. Figures 2 and 3 show the dependence of the peak stress on deformation temperature and strain rate, respectively. The classic interdependence of the peak stress, deformation temperature and strain rate can be seen, i.e. the peak stress increases with the decrease of deformation temperature and increase of strain rate. The peak strain also increases with the decrease of deformation temperature. However, the peak strain does not increase with the increase of strain rate. For the range of deformation conditions employed, the peak stress as a function of deformation temperature and strain rate is analysed through a hyperbolic-sine Arrhenius-type equation (Yuan and Liu 2005):

$$\dot{\varepsilon} = A\left[\sin h\left(\alpha \cdot \sigma_{\mathrm{p}}\right)\right]^{n} \exp\left(-Q/RT\right), \tag{3}$$

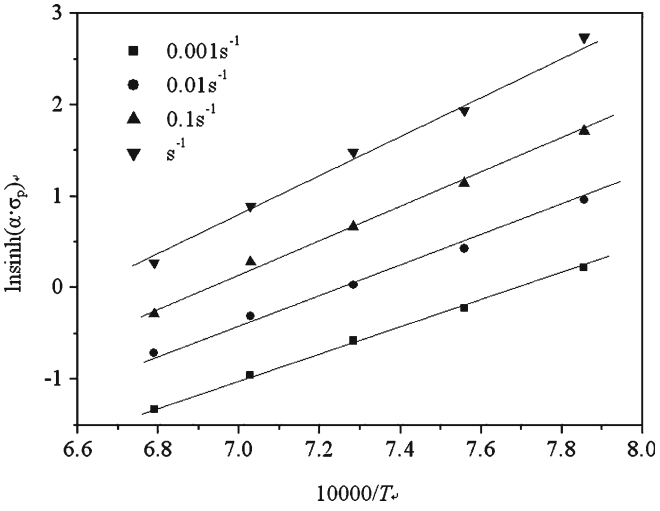

Figure 2. Relationship between hot deformation peak stress and temperature of Fe–24Ni–11Cr–1Mo–3Ti superalloy.

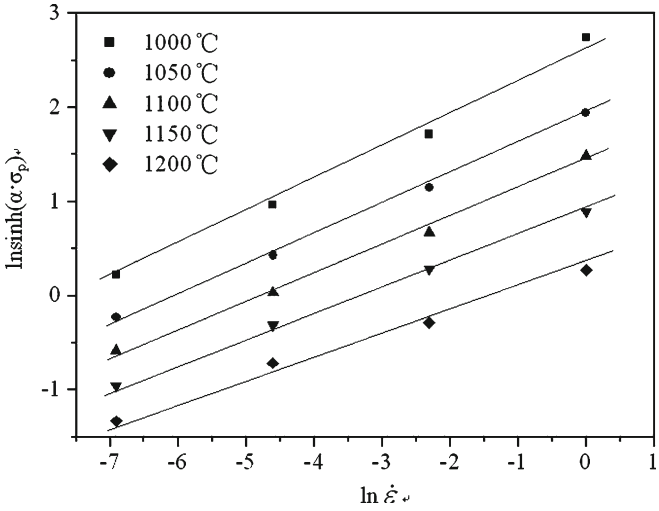

Figure 3. Relationship between hot deformation peak stress and strain rate of Fe–24Ni–11Cr–1Mo–3Ti superalloy.

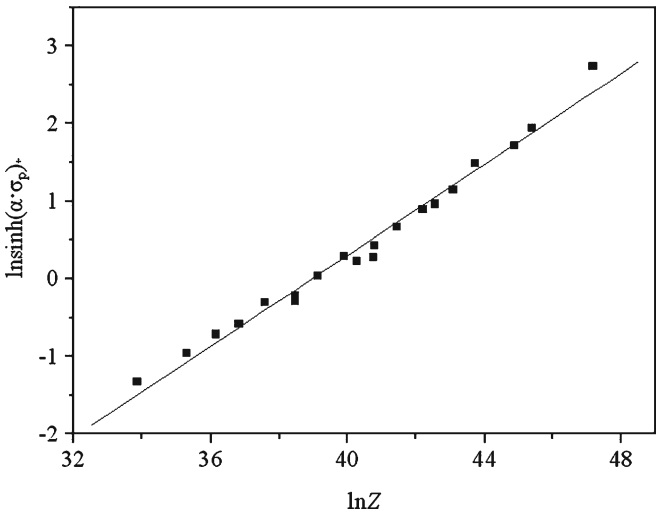

Figure 4. Relationship between hot deformation peak stress and Z parameter of Fe–24Ni–11Cr–1Mo–3Ti superalloy.

where A (s^{-1}) and α (MPa^{-1}) are materials constants, n a constant closely related to the strain rate, Q the activation energy of deformation (J/mol), R the universal gas constant, $\dot{\varepsilon}$ the strain rate (s^{-1}), T the deformation temperature in Kelvin and σ_{p} the peak stress (MPa). Equation (3) also can be rewritten as the following (Yuan and Liu 2005):

$$\ln \sin h\left(\alpha \cdot \sigma_{\mathrm{p}}\right) = -\frac{1}{n}\ln A + \frac{1}{n}\ln \dot{\varepsilon} + \frac{1}{n}\cdot\frac{Q}{RT}. \tag{4}$$

Linear statistical regression methods cannot be used directly to determine the values of α, A, n and Q because there are four constants of α, A, n and Q in (4). In order to calculate the values of A, n and Q, we first gave a value of α, and then calculated the values of A, n, Q and the residual sum of squares by fitting the experimental data. The residual sum

of squares should be as a function of α. The value of α was estimated from the minimum residual sum of squares to be $0{\cdot}012$ MPa^{-1}. The value of α represents the stress reciprocal upon which the material changes from power to exponential stress dependence. After the optimum value of α was determined, the values of A, n and Q were calculated as:

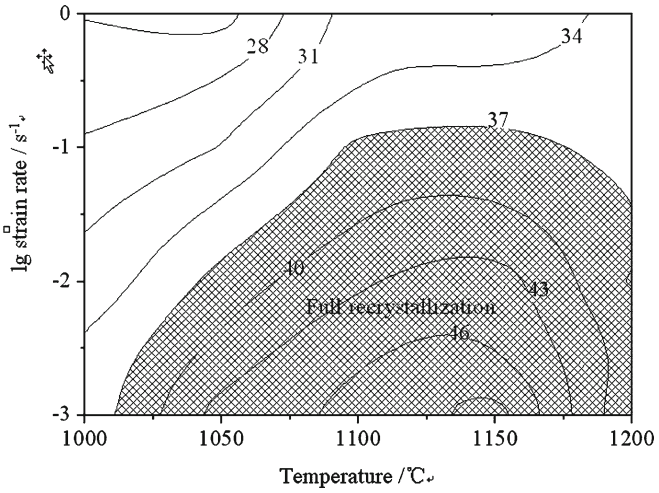

Figure 5. Processing map for Fe–24Ni–11Cr–1Mo–3Ti superalloy at a strain of 0·7, the numbers represent percent efficiency of power dissipation. Shaded region corresponds to full recrystallization.

$A = 3{\cdot}205 \times 10^{14}$ s^{-1}, $n = 3{\cdot}412$ and $Q = 499$ kJ/mol. Thus, (3) can be expressed as:

$$\dot{\varepsilon} = 3{\cdot}205 \cdot 10^{14} \left[\sin h \left(\alpha \cdot \sigma_p\right)\right]^{3{\cdot}412} \exp\left(-\frac{499000}{RT}\right).$$

The temperature compensated strain rate parameter or the Zener–Hollomon parameter is defined as (Raj 1981; Srinivasan and Prasad 1995; Seshacharyulu *et al* 2000; Park *et al* 2002):

$$Z = \dot{\varepsilon} \exp\left(\frac{Q}{RT}\right). \tag{5}$$

The variation in flow stress with Zener–Hollomon parameter for the superalloy is plotted in figure 4. It is seen that in the region of temperatures and strain rates considered, the rate equation is valid.

3.3 *Processing maps*

The power dissipation maps are continuum maps and can be interpreted in terms of the microstructural processes. These maps reveal the limiting temperature and strain rate conditions for the occurrence of fracture and instabilities during the deformation of materials. Generally, at lower temperatures and higher strain rates, void formation at hard particles occurs, while at higher temperatures and lower strain rates,

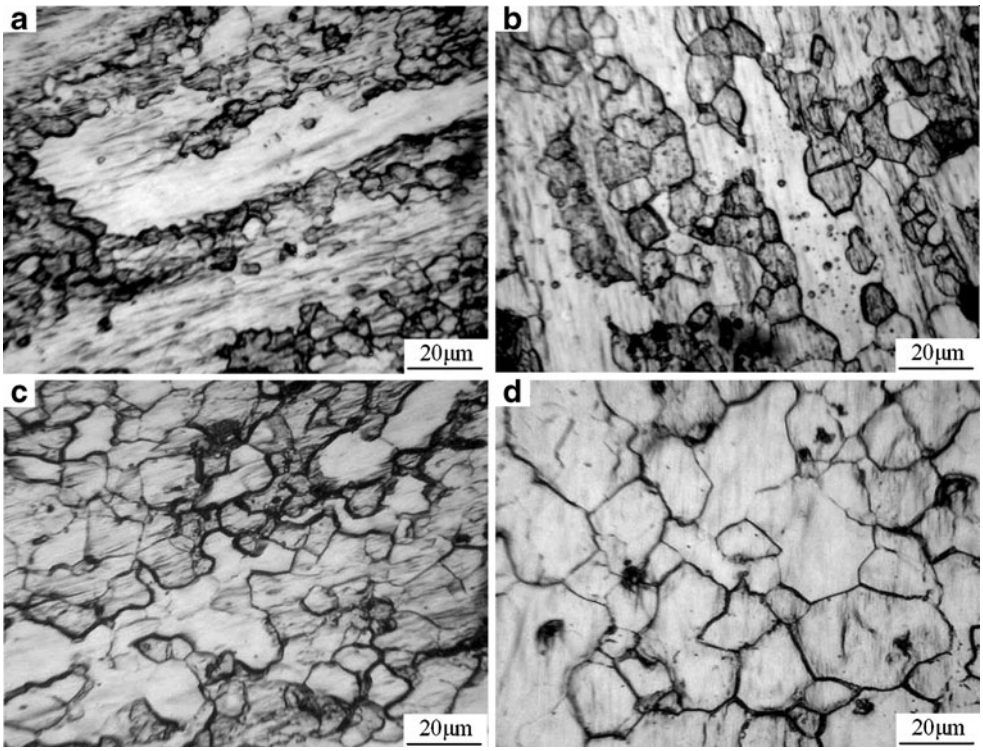

Figure 6. Typical microstructure characteristics of hot deformed Fe–24Ni–11Cr–1Mo–3Ti superalloy under different conditions: (**a**) deformed at 1000°C and 0·001/s^{-1}, (**b**) deformed at 1050°C and 0·1/s^{-1}, (**c**) deformed at 1050°C and 0·01/s^{-1} and (**d**) deformed at 1100°C and 0·1/s^{-1}.

wedge cracking occurs at grain boundary triple junctions. At very high strain rates, instability due to adiabatic shear band formation is the likelihood. The regime marked by the limiting conditions for these processes is termed "safe" for processing, and in this regime the processes of dynamic recovery (lower temperatures and strain rates) and dynamic recrystallization (higher temperatures and strain rates) occur. Both dynamic recovery and dynamic recrystallization are desirable processes during hot working of a uniform billet, to keep the flow stresses and rates of work hardening considerably low. In fact, dynamic recrystallization was shown to effectively expand the safe working zone by raising the upper bound for cavity nucleation at hard particle boundaries and moving lower bound for wedge crack initiation at grain boundary triple junction (Srinivasan and Prasad 1995; Somani *et al* 1995; Seshacharyulu *et al* 2000).

Typical processing maps generated in the temperature range 1000–1200°C and strain rate range 0·001–1·0 s^{-1} at a strain of 0·7 are shown in figure 5. The contours represent constant efficiencies of power dissipation expressed in percent. At other strains, the nature of the map is not significantly different from that given in figure 5. The maps obtained at strain of 0·1, 0·2, 0·3, 0·4, 0·6 and 0·7 are essentially similar to that obtained at a strain of 0·7, indicating that strain does not have a significant influence on it. The maps exhibit a clear domain with its peak efficiency at about 1150°C and 0·001 s^{-1}, and the domain has its peak efficiency at about 40–48% for the alloy in the strain range of 0·1–0·7.

The domain observed in the processing map is generally identified by correlating the efficiency variation with temperature and strain rate. The microstructure changes that occur in the deformed specimens also give evidence regarding the particular mechanism dominating in the domain. According to the atomistic processing map of Raj (1981), the observed domain may correspond either to superplasticity or dynamic recrystallization. The efficiency of power dissipation for superplasticity is generally very high (>60%). This is not observed in the map since the peak efficiency is only about 48%. In view of the observation, the domain observed does not represent superplastic deformation. So the domain in the processing map can be interpreted in terms of dynamic recrystallization, on the basis of hot deformation microstructural observation (figure 6), the full recrystallization region can be identified in the processing map at a strain of 0·7 (figure 5).

4. Conclusions

Hot compression testing of a Fe–24Ni–11Cr–1Mo–3Ti superalloy was conducted at various temperatures from 1000–1200°C under strain rates from 0·00–1 s^{-1} using processing maps. The following conclusions are drawn.

(I) Hot deformation equation is given to characterize the dependence of peak stress on temperature and strain rate. Hot deformation apparent activation energy of the superalloy is about 499 kJ/mol.
(II) The processing maps of the Fe–24Ni–11Cr–1Mo–3Ti superalloy obtained in a strain range of 0·1–0·7 are essentially similar. The maps exhibit a clear domain with its peak efficiency at about 1150°C and 0·001 s^{-1}, and the domain has its peak efficiency at about 40–48% in a strain range of 0·1–0·7. On the basis of hot deformation microstructural observation, the full recrystallization region is identified in the processing map at a strain rate of 0·7.

References

Balasubrahmanyam V V and Prasad Y V R K 2002 *Mater. Sci. Eng.* **A336** 150
Chakravartty J K, Dey G K and Banerjee S 1995 *J. Nucl. Mater.* **218** 247
Kusabiraki K, Amada E and Ooka T 1996 *ISIJ Int.* **36** 208
Kusabiraki K, Amada E, Ooka T and Saji S 1997 *ISIJ Int.* **37** 80
Kusabiraki K, Tsujino H and Saji S 1998 *ISIJ Int.* **38** 1015
Omar A A, Cabrera J M and Prado J M 1996 *Scr. Mater.* **34** 1303
Park N, Yeom J and Na Y 2002 *J. Mater. Process Technol.* **130–131** 540
Raj Rishi 1981 *Metall. Trans.* **A12** 1981
Seshacharyulu T, Medeiros S C and Morgan J T 2000 *Mater. Sci. Eng.* **A279** 289
Somani M C, Birla N C and Prasad Y V R K 1995 *J. Mater. Process Technol.* **52** 225
Srinivasan N and Prasad Y V R K 1995 *J. Mater. Process Tech.* **51** 171
Yuan H and Liu W C 2005 *Mater. Sci. Eng.* **A408** 281